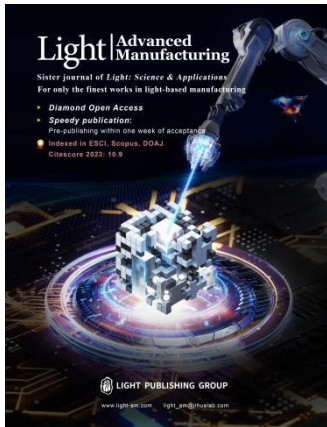


Accepted Article Preview: Published ahead of advance online publication



Development of a Surface Position Evaluation Method for Polyhedral Freeform Prisms

Tomofumi Morishita, Tatsuya Sakuma, Koji Handa and Akihiko Sugino

Cite this article as: Tomofumi Morishita, Tatsuya Sakuma, Koji Handa and Akihiko Sugino. Development of a Surface Position Evaluation Method for Polyhedral Freeform Prisms. *Light: Advanced Manufacturing* accepted article preview article preview 12 February, 2026; doi: 10.37188/lam.2026.034

This is a PDF file of an unedited peer-reviewed manuscript that has been accepted for publication. LAM are providing this early version of the manuscript as a service to our customers. The manuscript will undergo copyediting, typesetting and a proof review before it is published in its final form. Please note that during the production process errors may be discovered which could affect the content, and all legal disclaimers apply.

Received 02 July 2025; revised 17 January 2026; accepted 09 February 2026;
Accepted article preview online 12 February 2026

Development of a Surface Position Evaluation Method for Polyhedral Freeform Prisms

Tomofumi Morishita^{1,2}, Tatsuya Sakuma¹, Koji Handa¹, Akihiko Sugino¹

¹ Panasonic Production Engineering Co., Ltd.,
2-7 Matusba-cho, Kadoma city, Osaka, Japan, 571-0056

² Panasonic Corporation of China,
Panasonic Operation Excellence China & Northeast Asia Company,
No.300 Zhongnan street, SIP, Suzhou, Jiangsu, China, 215123

Abstract

With the rapid growth of extended-reality (XR) devices, simultaneously achieving long optical path length and miniaturization has become a central challenge in optical system design. One promising approach is to employ optical designs that utilize multiple internal reflections in a prism to extend the path length within a compact volume.

The prisms targeted in this study are polyhedral elements composed of three or more optical surfaces including freeform surfaces, in which two lateral faces are mutually parallel. A representative example is a triangular prism whose optical faces are replaced by freeform surfaces. Because such prisms contain multiple reflecting faces, their inter-surface positional relationships must be formed and maintained with high accuracy; consequently, metrology capable of precise evaluation of face-to-face position is indispensable for production.

Since 2002, Panasonic has introduced to the market inter-surface misalignment evaluation of lens surfaces using the ultra-high-accuracy three-dimensional profilometer UA3P, contributing to higher-precision camera modules. Building on that platform, the present work develops a new measurement method that extends the UA3P system to prisms with multiple reflecting faces, enabling spatial registration to be evaluated with an accuracy of 0.2–0.3 μm .

The developed system shows strong correlation with existing methods and validated repeatability, demonstrating its suitability for high-precision manufacturing and quality assurance of optical elements, including prisms for XR devices.

Keywords: XR (extended reality) devices; polyhedral prism; freeform surface; high-precision alignment; three-dimensional shape metrology; Ultra-high-accurate 3D profilometer (UA3P); optical component manufacturing; quality assurance.

1. Introduction

The market for extended-reality (XR) devices has expanded in recent years, and many optical manufacturers are actively developing new products. A 2021 market survey by Fuji-Kimera forecasts long-term growth in virtual-reality (VR), augmented-reality (AR), and mixed-reality (MR) devices [1]. By contrast, a Reuters report summarizing International Data Corporation (IDC) indicates sluggish demand over 2022–2024, with renewed expansion expected from 2026 onward [2]. From a long-term industry perspective, establishing mass-production capability for XR optics is therefore essential.

To realize higher-fidelity displays, direct-on-screen rendering architectures are being investigated. In such systems, a high-brightness RGB laser and a MEMS mirror enable wide-area image drawing; however, achieving a large scanned field typically requires a long propagation distance between the laser output and the MEMS mirror. To reconcile this requirement with compact form factors, polyhedral optical prisms that fold the beam path by multiple internal reflections are considered.

The prisms of interest comprise multiple optical faces—including freeform surfaces—and include configurations in which lateral faces are mutually parallel. The relative positions of these faces must be formed and maintained with high accuracy, necessitating metrology capable of precise inter-surface positional evaluation. In particular, for prisms incorporating freeform, more advanced evaluation techniques are required than for simple triangular prisms composed solely of planar faces that can be measured by generic three-dimensional measuring machines.

Manufacturing of polyhedral prisms with freeform geometry has been reported—for example, monolithic freeform fabrication by Optimax Systems Inc. in 2017 [3]. For XR applications, however, the required component size is on the order of a few millimeters,

and reports on the fabrication and metrology of small-scale freeform prisms in this regime remain scarce. Moreover, the optics industry requires standardized measurement methods suitable for high-volume production.

Since the 1990s, Panasonic has deployed the Ultra-high Accurate 3D Profilometer (UA3P), contributing to higher-quality optical devices. UA3P combines high-accuracy three-dimensional coordinate metrology with a low-force contact probe to enable absolute coordinate measurement, and—via comparison with mathematical reference surfaces—supports high-precision evaluation not only of rotationally symmetric profiles but also of freeform surfaces. According to [4], the UA3P-4000 used in this work attains a standard uncertainty of 30 nm.

In optical characterization, evaluation of surface figure and inter-surface decenter (axis misalignment) is standard. The same holds for polyhedral prisms, where both surface shape and the positional relationship between optical centers are critical. Building on UA3P-based coordinate metrology, Panasonic proposed an inter-surface decenter evaluation technique in 2002 [5], which has contributed to higher-precision camera modules. Subsequently, a method was developed to evaluate six-degree-of-freedom (6-DoF) misalignment, including twist between freeform surfaces [6].

In this paper, we extend these techniques and validate a surface-position evaluation method for polyhedral optical systems incorporating freeform.

2. Experimental Methods

2-1. Measurement System Overview

The UA3P-4000 used in this study is equipped with a three-axis, independently referenced laser interferometric length-measuring system common to the UA3P series, with a configuration that minimizes Abbe error (Fig. 1). Despite being contact-type, the instrument is equipped with a probe that achieves an ultra-low measuring force of 0.05 mN, enabling high-accuracy acquisition of three-dimensional shape coordinates.

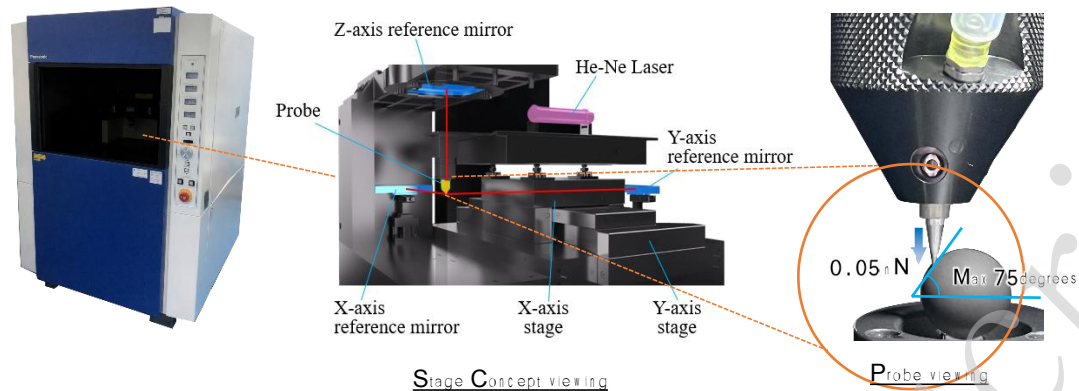


Fig.1 UA3P structure concept

The UA3P series provides an automatic six-axis (6-DoF) coordinate transformation (“alignment”) based on least-squares fitting of the measured coordinates to the target design equation, thereby evaluating deviations from the ideal surface (Fig. 2). In addition, the design surface to be evaluated can be programmed in C++, allowing high-precision measurement and evaluation against analytical reference surfaces even for complex geometries that include freeform surfaces.

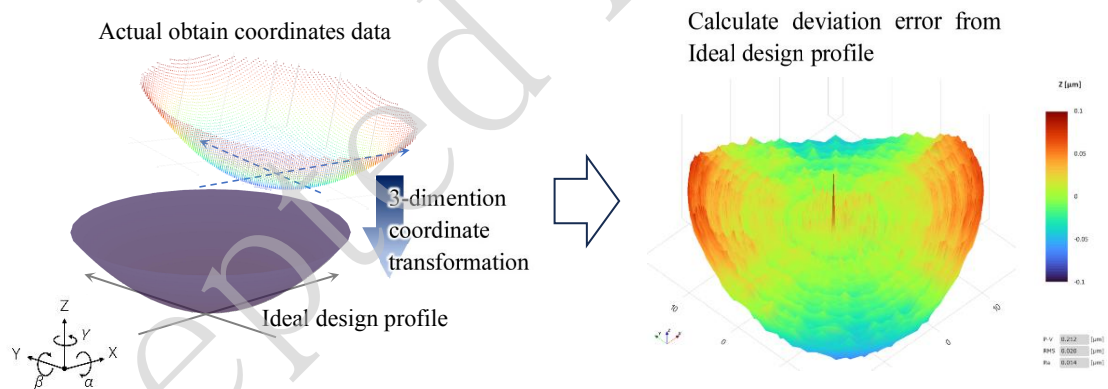


Fig.2 Work shape evaluation function overview

2-2. Consistency Check with the Conventional System

2-2-1. Overview of Inter-surface Evaluation for Rotationally Symmetric Aspheres

Since 2002, the UA3P series has supported an evaluation method—using the fixture

shown in Fig. 3 and the evaluation system in Fig. 5—for inter-surface optical-axis tilt, decenter, and center thickness of rotationally symmetric aspheric lenses.

Because of its mechanical configuration, UA3P fundamentally measures from the top side of the workpiece. Accordingly, inter-surface decenter evaluation requires the use of the fixture in Fig. 3: the front and back surfaces are measured separately, and the datasets are synthesized in software to compute positional misalignment. The fixture embeds standard spheres A, B, and C, which are measurable from both sides.

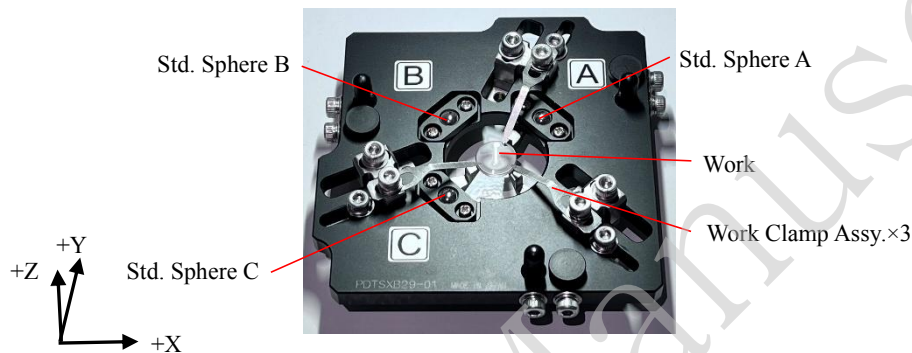


Fig.3 Standard decenter/tilt measurement fixture

The measurement procedure is as follows: measure the standard spheres and the workpiece from the fixture's first side (1st side), flip the fixture, and measure them again from the second side (2nd side).

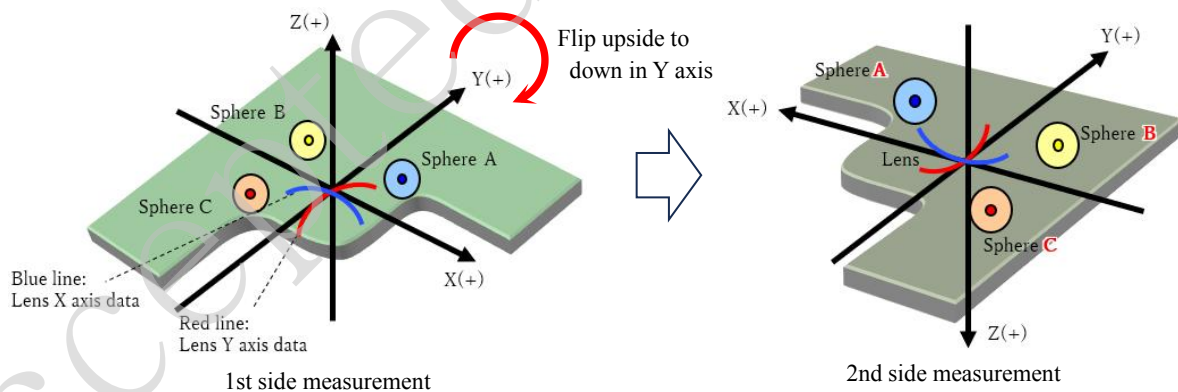


Fig.4 Measurement method of decenter/tilt measurement

The two coordinate frames are then synthesized using the centers of spheres A, B, and C. Finally, the normal vector $N1$ obtained from the reference (standard) surface and the normal vector $N2$ from the evaluation surface are compared to determine decenter, tilt, and center thickness (Fig. 5).

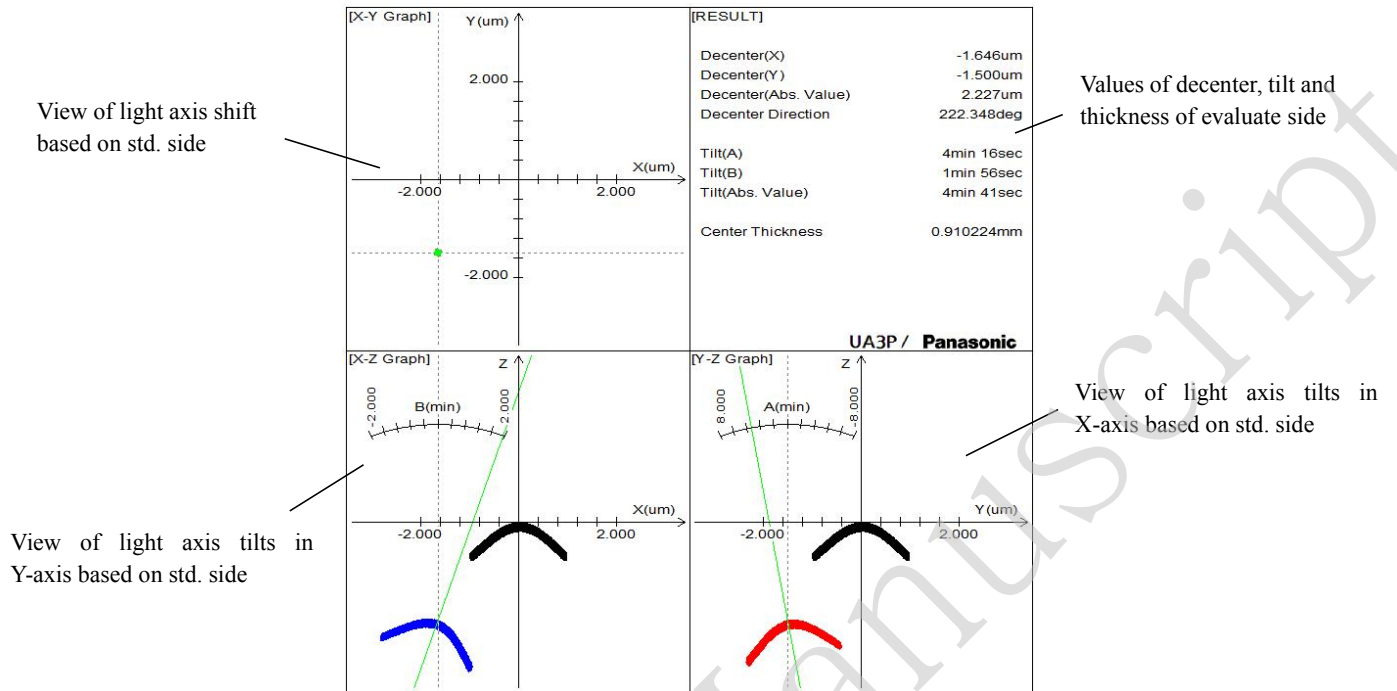


Fig.5 Decenter bi-aspherical lens evaluation system

2-2-2. Description of the Dataset for System Verification

We extended the conventional method for rotationally symmetric aspheres to enable evaluation of decenter, tilt, and twist between freeform surfaces; this method is referred to as the '22 algorithm. Its validation is reported in Ref. 6.

In the present work, the measurement dataset from Ref. 6 is re-evaluated using our newly developed system (hereafter the '24 algorithm), and the correlation between the two systems is assessed to verify effectiveness.

In Ref. 6, the workpiece in Fig. 6 was mounted in the fixture of Fig. 3, and tilt, decenter, and center thickness between the 1st and 2nd Polynomial Parts were measured five times each in repeated trials. The twist angle was evaluated twelve times by comparing the physical angle computed from UA3P measurements of a side reference plane on the workpiece with the angle computed by the '22 algorithm from the two Polynomial Parts. The optical prescriptions and boundary conditions are given in Fig. 7 and Tables 2-1 and 2-2, and the measurement conditions in Tables 2-3 and 2-4. The workpiece material was STAVAX, fabricated by diamond turning.

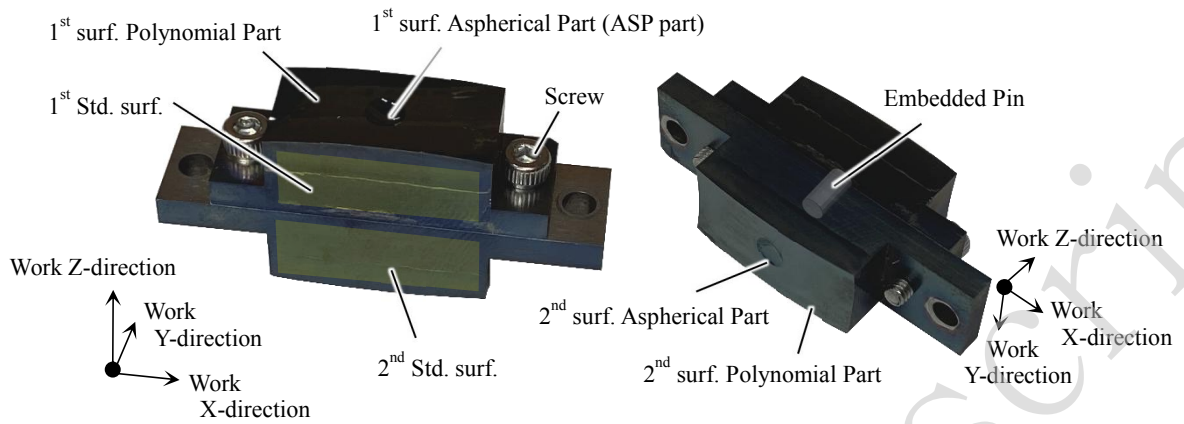


Fig.6 Workpiece structure for bi-freeform evaluation

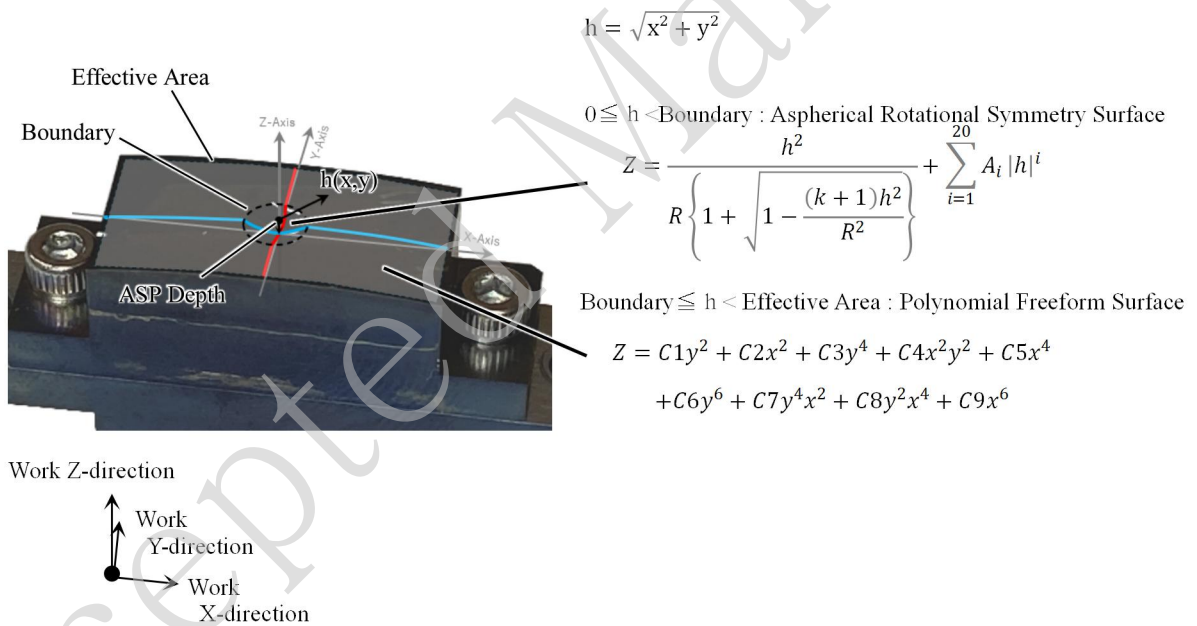


Fig.7 Design Structure of the workpiece

Table 2-1 Design equations parameters

Aspheric part		Polynomial Freeform	
R	-4.00270840	C1	-0.0052730
k	0.150	C2	0.0159710
A4	-0.0070	C3	-1.0440E-05
		C4	-2.3290E-08
		C5	3.0110E-09
		C6	-1.0120E-10
		C7	9.4910E-13
		C8	-4.7620E-12
		C9	-1.0800E-13

Table 2-2 Polynomial + Aspheric part shape boundary conditions

Boundary Radius	$\varphi 1.5\text{mm}$
Depth of aspheric part	-0.1711566mm
Freeform part Effective Area	20.0×8.0mm square

Table2-3 ASP + Polynomial part surface measurement conditions

Scan Range	Method	Scan Shift	Speed	Data Pitch
XY:18×8mm	Raster scan on Surface	0.4mm	1.2mm/s	0.01mm

Table2-4 Std. Sphere embedded in the fixture (ref. Fig.3) axis measurement conditions

Scan Range	Method	Speed	Data Pitch
±1.6mm	Axes Meas.	0.3mm/s	0.001mm

2-2-3. Comparative Results Between Systems

The '22 algorithm is limited to configurations in which the two optical surfaces face each other across the workpiece. It is therefore not applicable when the optical surfaces are arranged with an out-of-plane rotation of 90°. In contrast, the '24 algorithm augments the processing with automatic synthesis using Euler angles for arbitrary triplets of points in space, and was developed as a hybrid with the conventional approach.

The verification shows that, for all metrics—decenter (Table 2-5), tilt (Table 2-6), center thickness (Table 2-7), and twist angle (Table 2-8 and Fig. 8)—the differences between the two algorithms are within practical tolerances. Values for the '22 algorithm are quoted from Ref. 6.

Table2-5 Comparison decenter between '22 algorithm and '24 algorithm

Decenter	1st	2nd	3rd	4th	5th	Average
'22 Algorithm (μm)	11.368	11.196	11.424	11.369	11.064	11.284
'24 Algorithm (μm)	11.339	11.176	11.396	11.339	11.401	11.330
Difference (μm)	-0.029	-0.020	-0.028	-0.030	0.337	0.046

Table2-6 Comparison tilt between '22 algorithm and '24 algorithm

Tilt	1st	2nd	3rd	4th	5th	Average
'22 Algorithm (min. angle)	0.383	0.383	0.383	0.367	0.217	0.347
'24 Algorithm (min. angle)	0.398	0.393	0.391	0.383	0.391	0.360
Difference (min.angle)	0.015	0.009	0.007	0.017	0.175	0.013

Table2-7 Comparison center of thickness between '22 algorithm and '24 algorithm

Center of thicknes	1st	2nd	3rd	4th	5th	Average
'22 Algorithm (mm)	16.048	16.048	16.048	16.048	16.048	16.048
'24 Algorithm (mm)	16.048	16.048	16.048	16.048	16.048	16.048
Difference (mm)	0.000	0.000	0.000	0.000	0.000	0.000

Table2-8 Comparison twist angle of physical angle, '22 algorithm and '24 algorithm

Physical angle	Twist angle(min.angle)	
	'22 Algorithm	'24 Algorithm
0.0518	0.5500	0.5376
0.0518	0.5833	0.5726
0.0518	0.5667	0.5558
0.0518	0.5667	0.5687
0.0518	0.5667	0.5729
4.3585	3.7167	5.3947
12.0792	11.7667	11.7652
12.0792	11.7667	11.7755
24.1845	23.3667	23.3794
24.1845	23.3833	23.3937
46.5214	45.8333	45.8498
46.5214	45.8333	45.8526

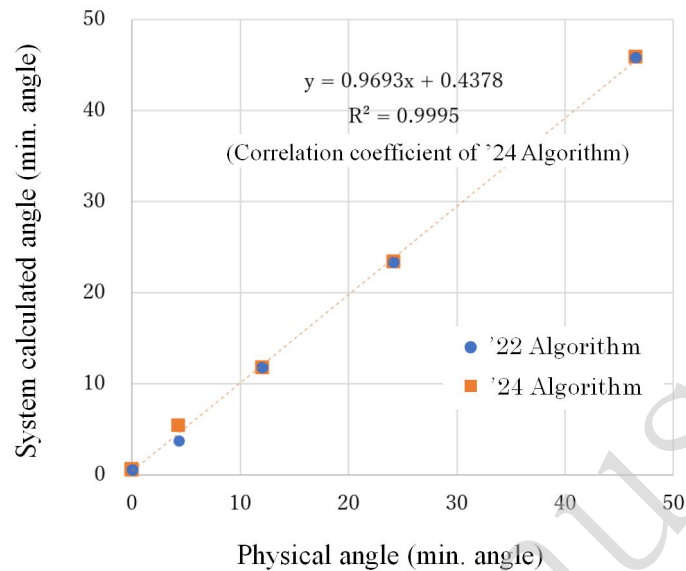


Fig.8 Graph of correlation between Physical angle and system calculated angle

3. Validation of Surface Position-Error Evaluation for Polyhedral Optical Systems

3-1. Overview of the Validation Workpiece

Because UA3P fundamentally assumes measurement from the top side of the workpiece, the conventional method using the fixture in Fig. 3 is not applicable to elements in which optical surfaces are arranged with an out-of-plane rotation of 90° . We therefore designed the validation workpiece shown in Fig. 9.

The workpiece measures $40 \times 16 \times 10$ mm and carries four optical faces on its periphery—two freeform surfaces and two planar faces. The material is STAVAX, and the part was fabricated by five-axis diamond turning. Freeform-2 is tilted, on average, by 38° out of plane relative to Freeform-1, and Plane-1 is rotated by approximately 90° out of plane with respect to Freeform-1. A notch is provided between Freeform-1 and Plane-1 as a positional reference.

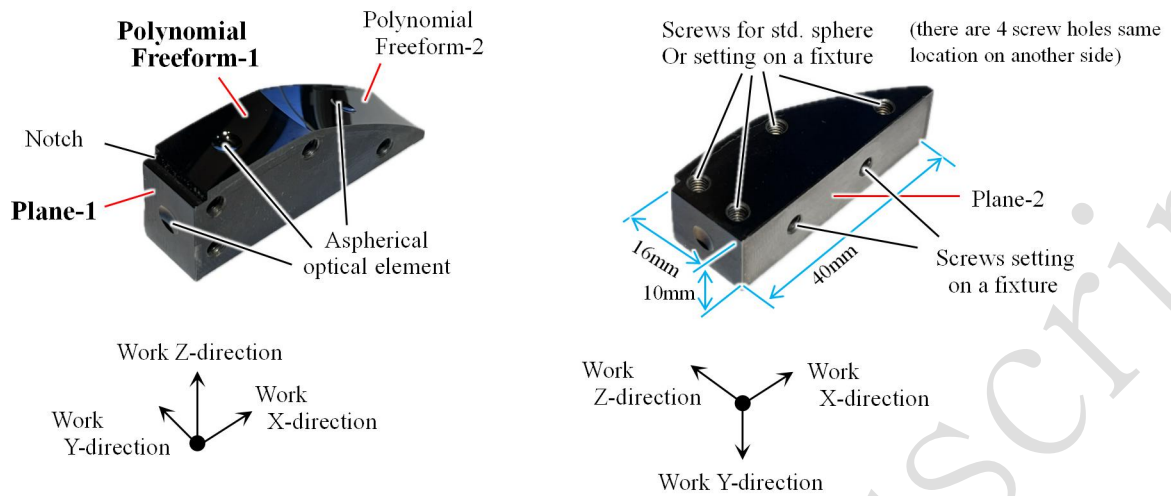


Fig.9 Polyhedral sample work overview

Standard spheres (ϕ 6.35 mm, silicon nitride, Grade 3) are mounted on ϕ 3 mm aluminum-alloy shafts and can be fixed into threaded holes on the side faces of the workpiece (Fig. 10).

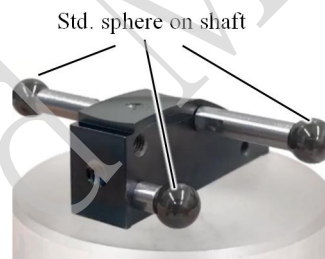


Fig.10 The work assembled std. sphere

By varying the shaft length and the mounting positions, the measurement posture can be changed while avoiding interference among the probe, workpiece, shafts, and spheres (Fig. 11).

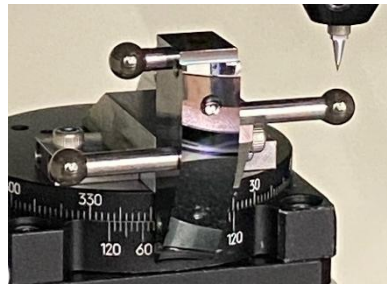


Fig.11 Example of work attitude for measurement

3-2. Optical Design Equations

Freeform-1 and the rotationally symmetric asphere reuse the equation structure employed in Fig. 7(see Fig. 12). For measurement convenience, the workpiece is installed with a 90° rotation about the Z-axis; however, the optical-surface program and the input coefficients remain unchanged. Machining is referenced to the center of the rotationally symmetric asphere, and the axes of the asphere and freeform regions are made coincident. The equation structure and parameters for Freeform-1 are listed in Tables 3-1 and 3-2, while the effective area of Plane-1, the parameters of the rotationally symmetric aspheric region contained within it, and the boundary conditions with the plane are presented in Tables 3-3, 3-4, and 3-5.

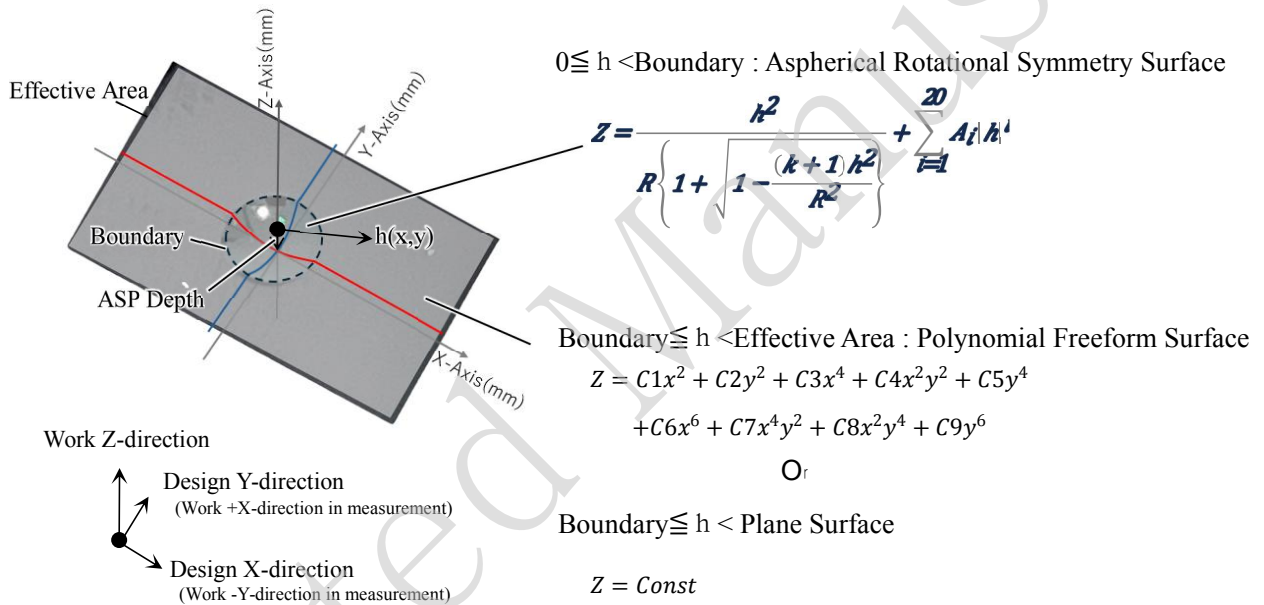


Fig.12 Design structure of freeform-1 part in Polyhedral work in Fig.9

Table3-1 Design equations parameters for Freeform-1 surface in Fig.9

Aspheric part		Polynomial Freeform	
R	-4.00270840	C1	-0.0052730
k	0.150	C2	0.0159710
A4	-0.0070	C3	-1.0440E-05
		C4	-2.3290E-08
		C5	3.0110E-09
		C6	-1.0120E-10
		C7	9.4910E-13
		C8	-4.7620E-12
		C9	-1.0800E-13

Table3-2 Aspherical part shape boundary conditions in Freeform-1 in Fig.9

Boundary Radius	$\phi 1.5\text{mm}$
Depth of aspheric part	-0.1740mm
Freeform-1 Effective Area	15.0×8.0mm square

Table3-3 Effective area of Plane-1 in Fig.9

Plane-1 Effective Area	8.0×8.0mm square
------------------------	------------------

Table3-4 Parameter of Aspherical part in Plane-1 surface in Fig.9

Aspheric part	
R	-4.00270840
k	0.150
A4	-0.0070

Table3-5 Aspherical part shape boundary conditions in Plane-1 in Fig.9

Boundary Radius	$\phi 1.5\text{mm}$
Depth of aspheric part	-0.32387mm

3-3. Measurement Procedure

The measurement proceeds as follows:

1. Plane-1 upward: perform centration using the rotationally symmetric asphere as the reference; measure the entire Plane-1 region and the three standard spheres.
2. Freeform-1 upward: again perform centration; measure the entire Freeform-1 region and the three standard spheres.

The measurement conditions for each surface and for the standard spheres are summarized in Tables 3-6, 3-7, and 3-8, respectively.

Table3-6 Plane-1 surface measurement conditions

Scan Range	Method	Scan Shift	Speed	Data Pitch
XY:8×8mm	Raster scan on Surface	0.2mm	3.0mm/s	0.005mm

Table3-7 Freeform-1 surface measurement conditions

Scan Range	Method	Scan Shift	Speed	Data Pitch
XY:14×8mm	Raster scan on Surface	0.2mm	3.0mm/s	0.005mm

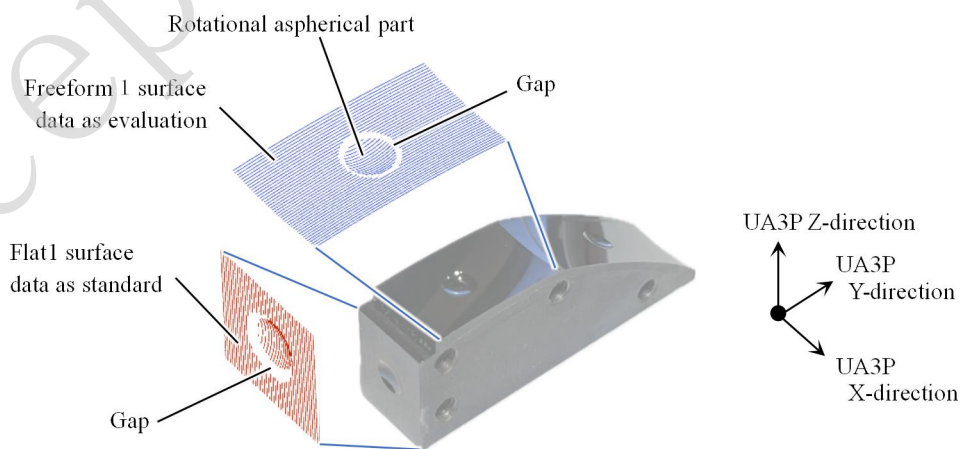
Table3-8 Std. Sphere on an aluminum shaft (ref. Fig.10) axis measurement conditions

Scan Range	Method	Speed	Data Pitch
±1.6mm	Axes Meas.	0.3mm/s	0.001mm

4. Experimental Results and Discussion

4-1. Relationship Between the UA3P Coordinate System and Data Position

Figure 13 illustrates the positional relationship between the reference and evaluation surface data of the workpiece. Figures 14 and 15 summarize the five-evaluation metrics. Gaps observed around the rotationally symmetric aspheric region originate from junctions that were not machined exactly according to the design; these were treated as noise and manually trimmed.

**Fig.13 Data location and coordinate system in UA3P (as 0 degree setting)**

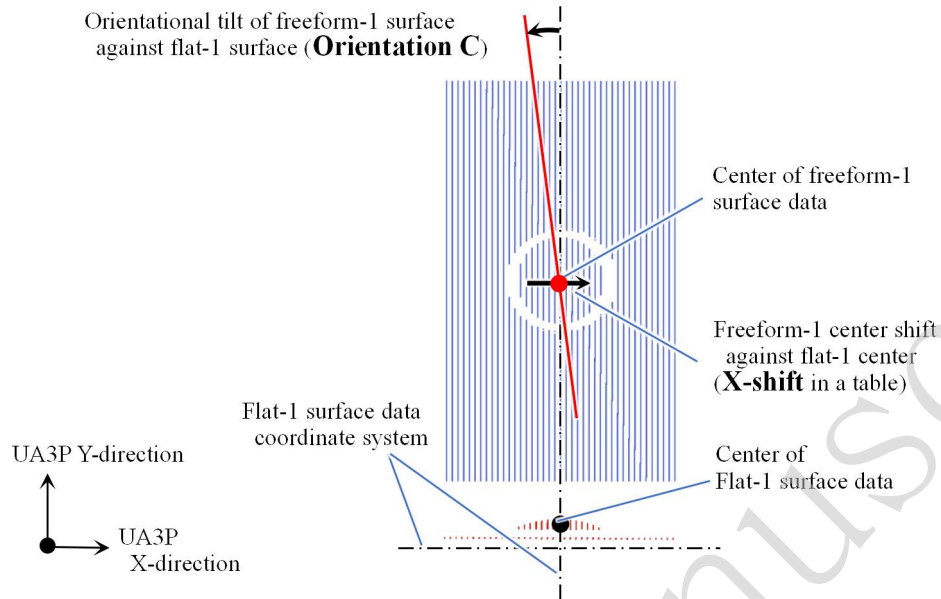


Fig.14 Data relation from Z top view in UA3P coordinate system

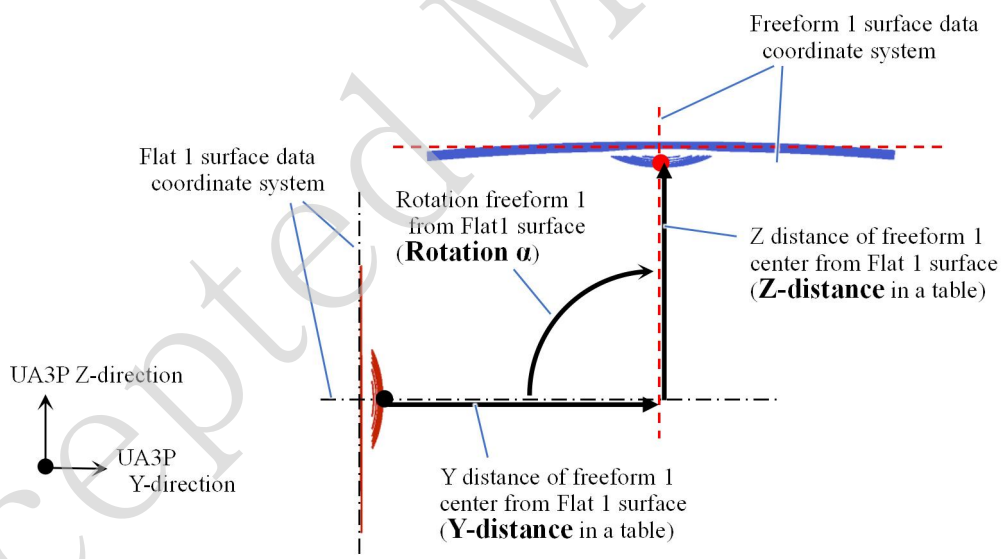


Fig.15 Data relation from X positive to X negative direction of fig.13

4-2. Repeatability at Installation Angle 0°

The workpiece was installed with an angle of approximately 0° relative to the machine coordinate system, and five repeated measurements were conducted. The results are listed in Table 4-1, showing good stability in both positional and angular evaluations. The sign convention of the tabulated values corresponds to the arrow directions indicated in Fig.14 and Fig.15

Table4-1 Freeform-1 surface position repeatability with setting angle 0degree.

Evaluation Metrics	1st	2nd	3rd	4th	5th	Ave.	Std. Dev.
X -shift[um]	-6.817	-7.041	-6.851	-6.785	-6.858	-6.870	0.089
Y-distance [um]	8385.095	8385.112	8385.109	8385.165	8385.160	8385.128	0.028
Z-distance [um]	6962.252	6962.311	6962.214	6962.150	6962.225	6962.230	0.053
Rotation α [min]	5399.030	5399.019	5399.029	5399.028	5398.991	5399.019	0.015
Orientation C [min]	1.067	1.062	1.044	1.057	1.052	1.056	0.008

4-3. Repeatability at Arbitrary Installation Angles

In industrial practice, the installation angle of a workpiece can vary from trial to trial. To evaluate robustness under such conditions, repeatability at arbitrary installation angles (Setting Rot.C) was tested, and results are summarized in Table 4-3. The sign convention of the tabulated values corresponds to the arrow directions indicated in Fig.14, Fig.15 and Fig.16. To avoid the risk of probe drop-off beyond the optical surface, the measurement range of Freeform-1 was restricted to 12 × 8 mm (Table 4-2). Other measurement conditions were identical to those in Tables 3-5 to 3-7.

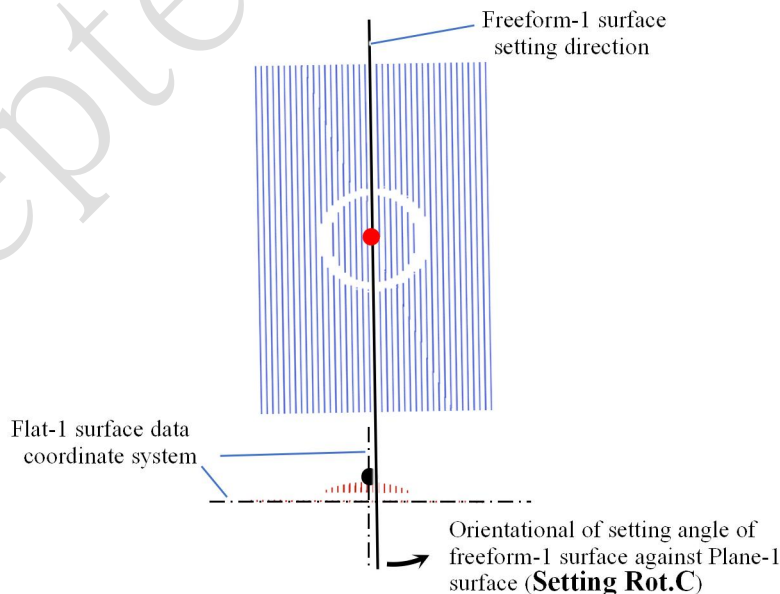


Fig.16 Setting angle overview from Z top view of Fig.13

Table4-2 Freeform-1 part surface measurement conditions with Setting Rot.C angle

Scan Range	Method	Scan Shift	Speed	Data Pitch
XY:12×8mm	Raster scan on Surface	0.2mm	3.0mm/s	0.005mm

Table4-3 Freeform-1 surface position repeatability with each of setting angles.

Representative Angle	0min	12min	24min	36min	48min	60min	75min	90min	Ave.	Std. Dev.	
Calculated Setting Rot. C [min]	-1.043	11.223	23.035	35.249	47.002	58.979	73.535	87.672			
Evaluation Metrics	X -shift[um]	-6.817	-7.395	-7.350	-7.893	-7.779	-7.886	-7.807	-7.847	-7.597	0.357
	Y-distance [um]	8385.095	8385.060	8384.982	8385.197	8385.253	8385.215	8385.203	8385.107	8385.139	0.087
	Z-distance [um]	6962.252	6962.137	6962.194	6962.054	6962.117	6962.134	6962.101	6962.023	6962.126	0.068
	Rotation α [min]	5399.030	5399.042	5399.016	5399.054	5399.049	5399.064	5399.054	5399.059	5399.046	0.015
	Orientation C [min]	1.067	1.050	1.022	0.849	0.866	0.848	0.859	0.814	0.922	0.098

5. Conclusions

This study extended the applicability of surface position evaluation beyond the conventional method (the '22 algorithm), which was restricted to face-to-face configurations, to include arbitrary orientations such as out-of-plane rotations of 90°.

Performance evaluations yielded the following findings:

- Consistency with the conventional method: High agreement was observed across all indices -decenter, tilt, center thickness, and twist.
- Accuracy and repeatability: Even in tests incorporating installation variability, repeatability was achieved within 0.357 μm deviation and 0.1 min angle rotation, demonstrating practical robustness and reliability.

Future work should address:

- Automated segmentation and processing of junction regions between optical surfaces.
- Implementation of automated measurement and evaluation routines compatible with industrial takt times.

Overall, the UA3P-based surface position evaluation method has established repeatability on the order of 0.3 μm , making it a promising candidate as a standard metrology process for polyhedral freeform prisms. This advancement is expected to make a substantive contribution to high-yield manufacturing and reliability assurance of high-density optical prisms for XR devices.

6. Summary

Surface position evaluation of polyhedral prisms using the UA3P system was confirmed to exhibit stable repeatability. By feeding back the obtained inter-surface positional relationships into optical simulations and manufacturing process factors, further improvements in production efficiency can be expected.

Moreover, the method was demonstrated to be applicable to optical-axis evaluation and optical path-length simulation of lens-integrated triangular prisms (called Power Prism Fig. 17), which are anticipated to see increasing demand in smartphone applications.

These results indicate that the proposed approach will make a significant and practical contribution to the development and mass production of polyhedral freeform prism optics for industrial applications.

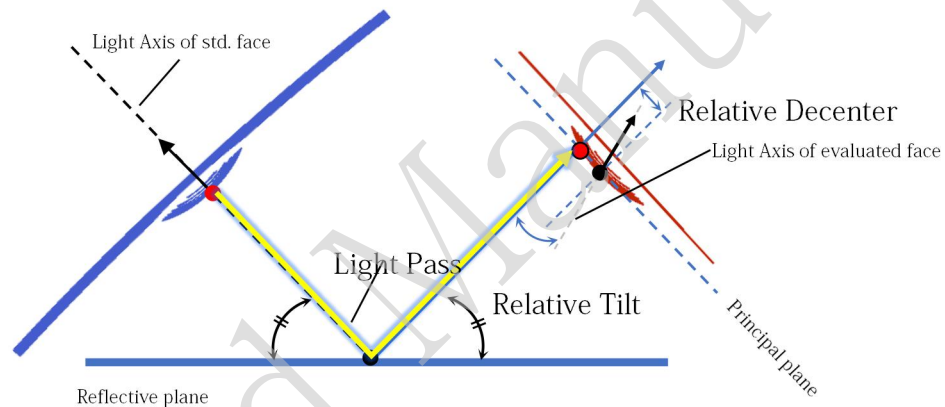


Fig.17 Example of application for power prism evaluation for smartphone

Reference

1. “the Imaging & Sensing Related Markets Survey 2021”, Amount of units based on survey of Fuji-Kimera Co.,Ltd. at <https://www.fcr.co.jp/report/203q06.htm> URL.
2. VR and AR headsets demand set to surge on AI, lower cost, IDC says, Reuters’s article for VR headsets demand, (2024). at <https://www.reuters.com/technology/artificial-intelligence/vr-ar-headsets-demand-set-to-surge-ai-lower-costs-idc-says-2024-09-16/> URL.
3. NASA. Freeform Monolithic Multi-Surface Telescope Manufacturing NASA mirror tech days 15 November 2017. (2017). at https://www.nasa.gov/wp-content/uploads/2024/04/optics-xrcf-techdays2017-36-optimax-freefor-monolithic-multi-surface-telescope-manufacturing.pdf?emrc=e58e1e&utm_source=chatgpt.com URL.

4. Kawashima, N. A Survey on Profile Measurement for Freeform Surfaces, Journal of the Society of Instrument and Control Engineers, vol.63,issue8,page499-507, (2024)
5. Takeuchi, H. & Kubo, K. About patent of decenter measurement system. (2002). at <https://www.j-platpat.inpit.go.jp/c1801/PU/JP-2002-071344/11/ja> URL.
6. Morishita, T. & Handa, K. & Sugino, A. Evaluation of decenter evaluation method between free-form lens surfaces, Proceedings of SPIE 12219, Polymer Optics and Molded Glass Optics: Design, Fabrication, and Materials, San Diego, California, United States: SPIE, 2022, 122190F doi:[10.1117/12.2635321](https://doi.org/10.1117/12.2635321).